



U-KAN Makes Strong Backbone for Medical Image Segmentation and Generation

Chenxin Li^{*}, Xinyu Liu^{*}, Wuyang Li^{*}, Cheng Wang^{*}, Hengyu Liu, Yixuan Yuan[✉]

The Chinese University of Hong Kong

Abstract

U-Net has become a cornerstone in various visual applications such as image segmentation and diffusion probability models. While numerous innovative designs and improvements have been introduced by incorporating transformers or MLPs, the networks are still limited to linearly modeling patterns as well as the deficient interpretability. To address these challenges, our intuition is inspired by the impressive results of the Kolmogorov-Arnold Networks (KANs) in terms of accuracy and interpretability, which reshape the neural network learning via the stack of non-linear learnable activation functions derived from the Kolmogorov-Arnold representation theorem. Specifically, in this paper, we explore the untapped potential of KANs in improving backbones for vision tasks. We investigate, modify and re-design the established U-Net pipeline by integrating the dedicated KAN layers on the tokenized intermediate representation, termed U-KAN. Rigorous medical image segmentation benchmarks verify the superiority of U-KAN by higher accuracy even with less computation cost. We further delved into the potential of U-KAN as an alternative U-Net noise predictor in diffusion models, demonstrating its applicability in generating task-oriented model architectures. These endeavours unveil valuable insights and sheds light on the prospect that *with U-KAN, you can make strong backbone for medical image segmentation and generation*. Project page: <https://yes-ukan.github.io/>.

1 Introduction

Over the past decade, numerous works have focused on developing efficient and robust segmentation methods for medical imaging, driven by the needs of computer-aided diagnosis and image-guided surgical systems [42, 44, 48, 51, 52, 77, 78]. Among these, U-Net [71] is a landmark work that initially demonstrated the effectiveness of encoder-decoder convolutional networks with skip connections for medical image segmentation [13, 43, 84, 90]. In recent years, UNet has become the backbone of nearly all leading medical image segmentation methods, and has also shown promising results in many image translation tasks. Additionally, recent diffusion models have utilized U-Net, training it to iteratively predict the noise to be removed in each denoising step.

Since the inception of U-Net [71], a series of crucial modifications have been introduced, especially in the subfield of medical imaging, including U-Net++[94], 3D U-Net[12], V-Net [60], and Y-Net [58]. U-NeXt [81] and Rolling U-Net[54] integrate a hybrid approach involving convolutional operations and MLP to optimize the efficacy of segmentation networks, enabling their deployment at point-of-care settings with limited resources. Recently, numerous transformer-based networks have been utilized to enhance the U-Net backbone for medical image segmentation. These networks

C. Li (♠♥♣♠), X. Liu (♠♥♣), W. Li (♥♣♠), C. Wang (♥♣) make equal contribution.
 ✉: Conceptualization ♥: Implementation ♣: Writing ♠: Visualization

have demonstrated effectiveness in addressing global context and long-range dependencies [24, 68]. Examples include Trans-UNet [9], which adopts ViT architecture [14] for 2D medical image segmentation using U-Net, and other transformer-based networks like MedT [80] and UNETR [23]. Although highly sophisticated, transformers tend to overfit when dealing with limited datasets, indicating their data-hungry nature [50, 79]. In contrast, structured state-space sequence models (SSMs) [16, 18, 67] have recently shown high efficiency and effectiveness in long-sequence modeling, and are promising solutions for long-term dependency modeling in visual tasks. For medical image segmentation, U-Mamba [56] and SegMamba [88] have proposed task-specific architectures with Mamba blocks respectively based on nn-UNet [32] and Swin UNETR [22], respectively, achieving promising results in various visual tasks and demonstrating the potential of SSMs in vision.

While existing U-shape variations have advanced in fine-trained medical scenarios, e.g., medical image segmentation, they still have fundamental challenges due to their sub-optimal kernel design and the unexplainable nature. Concretely, first, they typically employ conventional kernels* to capture the spatial dependence between local pixels, which are **limited to linearly modeling patterns** and relationships across different channels in latent space. This makes it challenging to capture complex nonlinear patterns. Such intricate nonlinear patterns among channels are prevalent in visual tasks, such as medical imaging, where images often have intricate diagnostic characteristics. This complexity implies that feature channels might possess varying clinical relevance, representing different anatomical components or pathological indicators. Second, they mostly conduct empirical network search and heuristic model design to find the optimal architecture, **ignoring the interpretability and explainability** in existing black-box U-shape models. In existing U-shape variations, this unexplainable property poses a significant risk in clinical decision-making, further preventing the truth-worth of diagnostic system design. Recently, Kolmogorov-Arnold Networks (KANs) have attempted to open the black box of conventional network structures with superior interpretability, revealing the great potential of white-box network research [64, 92]. Considering the excellent architecture properties merged in KANs, it makes sense to effectively leverage KAN to bridge the gap between the network’s physical attributes and empirical performance.

In this endeavor, we have embarked on the exploration of a universally applicable U-KAN framework, denoted as U-KAN, marking an inaugural attempt to integrate advanced KAN into the pivotal visual backbone of UNet, through a convolutional KAN mixed architectural style. Notably, adhering to the benchmark setup of U-Net, we employ a multilayered deep encoder-decoder architecture with skip connections, incorporating a novel tokenized KAN block at higher-level representations proximate to the bottleneck. This block projects intermediate features into tokens, subsequently applying the KAN operator to extricate informative patterns. The proposed U-KAN benefits from the alluring attributes of KAN networks in terms of non-linear modeling capabilities and interpretability, which distinguish it prominently within the prevalent U-Net architecture. Empirical evaluations on stringent medical segmentation benchmarks, both quantitative and qualitative, underscore U-KAN’s superior performance, outpacing established U-Net backbones with enhanced accuracy even without less computation cost. Our investigation further delves into the potentiality of U-KAN as an alternative U-Net noise predictor in diffusion models, substantiating its relevance in generating task-oriented model architectures. In a nutshell, U-KAN signifies a steady step toward the design that incorporates mathematics theory-inspired operators into efficient visual pipelines and foretells its prospects in extensive visual applications. Our contributions can be summarized as follows:

- We present the first effort to incorporate the advantage of emerging KAN to improve established U-Net pipeline to be more accurate, efficient and interpretable.
- We propose a tokenized KAN block to effectively steer the KAN operators to be compatible with the exiting convolution-based designs.
- We empirically validate U-KAN on a wide range of medical segmentation benchmarks, achieving impressive accuracy and efficiency.
- The application of U-KAN to existing diffusion models as an improved noise predictor demonstrates its potential in backboning generative tasks and broader vision settings.

*Such operations include convolution, Transformers, and MLPs, etc.

2 Related work

2.1 U-Net Backbone for Medical Image Segmentation

Medical image segmentation is a challenging task to which deep learning methods have been extensively applied and achieved breakthrough advancements in recent years [40, 49, 62, 71, 77]. U-Net [71] is a popular network structure for medical image segmentation. Its encoder-decoder architecture effectively captures image features. The CE-Net [20] further integrates a contextual information encoding module, enhancing the model’s receptive field and semantic representation capabilities. Unet++ [94] proposes a nested U-Net structure that fuses multi-scale features to improve segmentation accuracy. In addition to convolution-based methods, Transformer-based models have also gained attention. The Vision Transformer [14] demonstrates the effectiveness of Transformers in image recognition tasks. The Medical Transformer [80] and TransUNet [9] further incorporate Transformers into medical image segmentation, achieving satisfying performance. Moreover, techniques such as attention mechanism [76] and multi-scale feature fusion [31] are widely used in medical image segmentation tasks. 3D segmentation models like Multi-dimensional Gated Recurrent Units [2] and Efficient Multi-Scale 3D CNN [34] also yield commendable results. In summary, medical image segmentation is an active research field where deep learning methods have made significant progress. Recently, Mamba [18] has achieved a groundbreaking milestone with its linear-time inference and efficient training process by integrating selection mechanism and hardware-aware algorithms into previous works [19, 21, 57]. Building on the success of Mamba, for visual application, Vision Mamba [53] and VMamba [95] use bidirectional Vim Block and the Cross-Scan Module respectively to gain data-dependent global visual context. At the same time, U-Mamba [56] and other works [72, 88] show superior performance in medical image segmentation. As Kolmogorov–Arnold Network (KAN) [55] has been emerged as a promising alternative for MLP and demonstrates its precision, efficiency, and interpretability, we believe now is the right time to open up the exploration of its broader applications in vision backbones.

2.2 U-Net Diffusion Backbone for Image Generation

Diffusion Probability Models, a frontier category of generative models, have emerged as a focal point in the research domain, particularly in tasks related to computer vision [26, 69, 70]. Unlike other categories of generative models [7, 17, 35, 36, 61, 83], such as Variational Autoencoders (VAE) [36], Generative Adversarial Networks (GANs) [7, 17, 35, 93], and vector quantization methods [15, 82], diffusion models introduce a novel generative paradigm. These models employ a fixed Markov chain to map the latent space, fostering complex mappings that capture the intricate structure inherent in datasets. Recently, their impressive generative prowess, from high-level detail to diversity in generated samples, has propelled breakthrough progress in various computer vision applications, such as image synthesis [26, 70, 74], image editing [3, 11, 46, 59], image-to-image translation [11, 45, 73, 85], and video generation [6, 25, 27, 41]. Diffusion models consist of a *diffusion process* and a *denoising process*. In the diffusion process, Gaussian noise is gradually added to the input data, eventually corroding it to approximate pure Gaussian noise. In the *denoising process*, the original input data is recovered from its noisy state through a learned sequence of inverse diffusion operations. Typically, convolutional U-Nets [71], the de-facto choice of backbone architecture, are trained to iteratively predict the noise to be removed at each denoising step. Diverging from previous work that focuses on utilizing pre-trained diffusion U-Nets for downstream applications, recent work has committed to exploring the intrinsic features and structural properties of diffusion U-Nets. Free-U investigates strategically reassessing the contribution of U-Net’s skip connections and backbone feature maps to leverage the strengths of the two components of the U-Net architecture. RINs [33] introduced a novel, efficient architecture based on attention for DDPMs. DiT [66] proposed the combination of pure transformer with diffusion, showcasing its scalable nature. In this paper, we demonstrate the potential of a backbone scheme integrating U-Net and KAN for generation, pushing the boundaries and options for generation backbone.

2.3 Kolmogorov–Arnold Networks (KANs)

The Kolmogorov-Arnold theorem [37] postulates that any continuous function can be expressed as a composition of continuous unary functions of finite variables, providing a theoretical basis for the construction of universal neural network models. This was further substantiated by Hornik et al. [28],

who demonstrated that feed-forward neural networks possess universal approximation capabilities, paving the way for the development of deep learning. Drawing from the Kolmogorov-Arnold theorem, scholars proposed a novel neural network architecture known as Kolmogorov-Arnold Networks (KANs) [29]. KANs consist of a series of concatenated Kolmogorov-Arnold layers, each containing a set of learnable one-dimensional activation functions. This network structure has proven effective in approximating high-dimensional complex functions, demonstrating robust performance across various applications. KANs are characterized by strong theoretical interpretability and explainability. Huang et al. [30] analyzed the optimization characteristics and convergence of KANs, validating their excellent approximation capacity and generalization performance. Liang et al. [47] further introduced a deep KAN model and applied it to tasks such as image classification. Xing et al. [87] deployed KANs for time series prediction and control problems. Despite these advancements, there has been a lack of practical implementations to broadly incorporate the novel neural network model of KAN, which has strong theoretical foundations, into general-purpose vision networks. In contrast, this paper undertakes an initial exploration, attempting to design a universal visual network architecture that integrates KAN and validates it on a wide range of segmentation and generative tasks.

3 Method

Architecture Overview Fig. 1 illustrates the overall architecture of the proposed U-KAN, following a two-phrase encoder-decoder architecture comprising a Convolution Phrase and a Tokenized Kolmogorov-Arnold Network (Tok-KAN) Phrase. The input image traverses the encoder, where the initial three blocks utilize convolution operations, followed by two tokenized MLP blocks. The decoder comprises two tokenized KAN blocks succeeded by three convolution blocks. Each encoder block halves the feature resolution, while each decoder block doubles it. Additionally, skip connections are integrated between the encoder and decoder. The channel count for each block in Convolution Phrase and Tok-KAN Phrase is respectively determined by hyperparameters as C_1 to C_3 and D_1 to D_2 .

3.1 KAN as Efficient Embedder

This research aims to incorporate Knowledge Aware Networks (KANs) into the UNet framework or, alternatively, to independently utilize KANs for medical image segmentation tasks. The basis of this approach is the proven high efficiency and interpretability of KANs as outlined in [55]. A Multi-Layer Perceptron (MLP) comprising K layers can be described as an interplay of transformation matrices W and activation functions σ . This can be mathematically expressed as:

$$\text{MLP}(\mathbf{Z}) = (W_{K-1} \circ \sigma \circ W_{K-2} \circ \sigma \circ \dots \circ W_1 \circ \sigma \circ W_0) \mathbf{Z}, \quad (1)$$

where it strives to mimic complex functional mappings through a sequence of nonlinear transformations over multiple layers. Despite its potential, the inherent obscurity within this structure significantly hampers the model’s interpretability, thus posing considerable challenges to intuitively understanding the underlying decision-making mechanisms.

In an effort to mitigate the issues of low parameter efficiency and limited interpretability inherent in MLPs, Liu *et al.* [55] proposed the Kolmogorov-Arnold Network (KAN), drawing inspiration from the Kolmogorov-Arnold representation theorem [38]. Similar to an MLP, a K -layer KAN can be characterized as a nesting of multiple KAN layers:

$$\text{KAN}(\mathbf{Z}) = (\Phi_{K-1} \circ \Phi_{K-2} \circ \dots \circ \Phi_1 \circ \Phi_0) \mathbf{Z}, \quad (2)$$

where Φ_i signifies the i -th layer of the entire KAN network. Each KAN layer, with n_{in} -dimensional input and n_{out} -dimensional output, Φ comprises $n_{in} \times n_{out}$ learnable activation functions ϕ :

$$\Phi = \{\phi_{q,p}\}, \quad p = 1, 2, \dots, n_{in}, \quad q = 1, 2, \dots, n_{out}, \quad (3)$$

The computation result of the KAN network from layer k to layer $k+1$ can be expressed in matrix form:

$$\mathbf{Z}_{k+1} = \underbrace{\begin{pmatrix} \phi_{k,1,1}(\cdot) & \phi_{k,1,2}(\cdot) & \dots & \phi_{k,1,n_k}(\cdot) \\ \phi_{k,2,1}(\cdot) & \phi_{k,2,2}(\cdot) & \dots & \phi_{k,2,n_k}(\cdot) \\ \vdots & \vdots & \ddots & \vdots \\ \phi_{k,n_{k+1},1}(\cdot) & \phi_{k,n_{k+1},2}(\cdot) & \dots & \phi_{k,n_{k+1},n_k}(\cdot) \end{pmatrix}}_{\Phi_k} \mathbf{Z}_k, \quad (4)$$

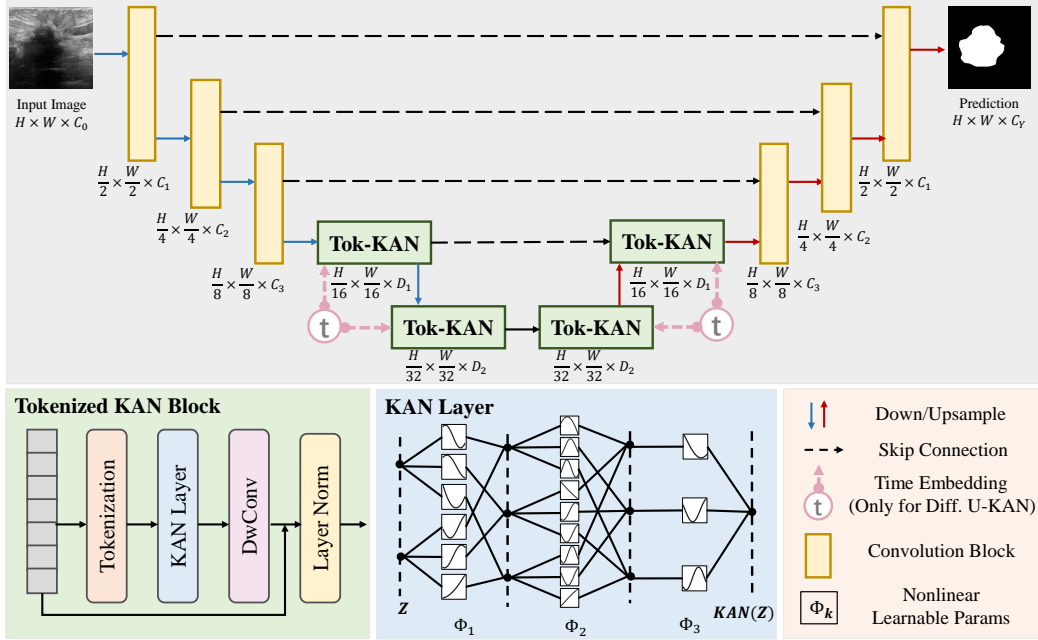


Figure 1: Overview of U-KAN pipeline. After feature extraction by several convolution blocks in Convolution Phrase, the intermediate maps are tokenized and processed by stacked Tok-KAN blocks in Tokenized KAN Phrase. The time embedding is only injected into the KAN blocks when applied for Diffusion U-KAN.

In conclusion, KANs differentiate themselves from traditional MLPs by using learnable activation functions on the edges and parametrized activation functions as weights, eliminating the need for linear weight matrices. This design allows KANs to achieve comparable or superior performance with smaller model sizes. Moreover, their structure enhances model interpretability without compromising performance, making them suitable for various applications.

3.2 U-KAN Architecture

3.2.1 Convolution Phrase

Each convolution block is constructed of a trio of components: a convolutional layer (Conv), a batch normalization layer (BN), and a ReLU activation function. We apply a kernel size of 3x3, a stride length of 1, and a padding quantity of 1. The convolution blocks within the encoder integrate a max-pooling layer with a pool window dimension of 2x2, while those housed in the decoder encompass a bilinear interpolation layer to magnify the feature maps. Formally, given an image $\mathbf{X}_0 = \mathbf{I} \in \mathbb{R}^{H_0 \times W_0 \times C_0}$, the output of each convolution block can be elaborated as:

$$\mathbf{X}_\ell = \text{Pool}(\text{Conv}(\mathbf{X}_{\ell-1})), \quad (5)$$

where $\mathbf{X}_\ell \in \mathbb{R}^{H_\ell \times W_\ell \times C_\ell}$ represents the output feature maps at ℓ -th layer. Given the configuration that there are L blocks in the Convolution Phrase, the final output is derived as \mathbf{X}_L .

3.2.2 Tokenized KAN Phrase

Tokenization In the tokenized KAN block, we first perform tokenization [10, 14] by reshaping the output feature of convolution phrase \mathbf{X}_L into a sequence of flattened 2D patches $\{\mathbf{X}_L^i \in \mathbb{R}^{P^2 \cdot C_L} | i = 1, \dots, N\}$, where each patch is of size $P \times P$ and $N = \frac{H_L \times W_L}{P^2}$ is the number of feature patches. We first map the vectorized patches \mathbf{x}_p into a latent D -dimensional embedding space using a trainable linear projection $\mathbf{E} \in \mathbb{R}^{(P^2 \cdot C_L) \times D}$, as:

$$\mathbf{Z}_0 = [\mathbf{X}_L^1 \mathbf{E}; \mathbf{X}_L^2 \mathbf{E}; \dots; \mathbf{X}_L^N \mathbf{E}], \quad (6)$$

The linear projection $\mathbf{E} \in \mathbb{R}^{(P^2 \cdot C_L) \times D}$ is implemented by a convolution layer with a kernel size of 3, as it is shown in [86] that a convolution layer is enough to encode the positional information and it actually performs better than the standard positional encoding techniques. Positional encoding techniques like the ones in ViT need to be interpolated when the test and training resolutions are not the same often leading to reduced performance.

Embedding by KAN Layer Given the obtained tokens, We pass them into a series of KAN layers ($N = 3$). Followed each KAN layers, the features are passed through a efficient depth-wise convolutional layer (DwConv) [8] and a batch normalization layer (BN) and a ReLU activation. We use a residual connection here and add the original tokens as residuals. We then apply a layer normalization (LN) [4] and pass the output features to the next block. Formally, the output of k -th Tokenized KAN block can be elaborated as:

$$\mathbf{Z}_k = \text{LN}(\mathbf{Z}_{k-1} + \text{DwConv}(\text{KAN}(\mathbf{Z}_{k-1}))), \quad (7)$$

where $\mathbf{Z}_k \in \mathbb{R}^{H_k \times W_k \times D_k}$ is the output feature maps at k -th layer. Given the setup that there are K blocks in the Tokenized KAN Phrase, the final output is derived as \mathbf{Z}_K . In our implementation, we set $L = 3$ and $K = 2$.

3.2.3 U-KAN Decoder

We follow the commonly used U-shaped architecture with dense skip connections to construct U-KAN. U-Net and its variations have demonstrated remarkable efficiency in medical image segmentation tasks [39, 89, 91]. This architecture leverages skip connections for the recovery of low-level details and employs an encoder-decoder structure for high-level information extraction.

Given skip-connected feature \mathbf{Z}_k from layer- k in KAN Phrase and feature \mathbf{Z}'_{k+1} from the last up-sample block, the output feature \mathbf{Z}'_k of k -th up-sample block is:

$$\mathbf{Z}'_k = \text{Cat}(\mathbf{Z}'_{k+1}, (\mathbf{Z}_k)), \quad (8)$$

where $\text{Cat}(\cdot)$ denotes the feature concatenation operation. Likewise, given skip-connected feature \mathbf{X}_ℓ from layer- ℓ in Convolution Phrase and feature $\mathbf{X}'_{\ell+1}$ from the last up-sample block, the output feature \mathbf{X}'_ℓ of ℓ -th up-sample block is:

$$\mathbf{X}'_\ell = \text{Cat}(\mathbf{X}'_{\ell+1}, (\mathbf{X}_\ell)), \quad (9)$$

In the context of semantic segmentation tasks, the final segmentation map can be derived from the output feature maps $\mathbf{X}'_0 \in \mathbb{R}^{H_0 \times W_0 \times C_Y}$ at layer-0, where C_Y is the number of semantic categories and \mathbf{Y} denotes the ground-truth segmentation and. As a result, the segmentation loss can be:

$$\mathcal{L}_{\text{Seg}} = \text{CE}(\mathbf{Y}, \text{U-KAN}(\mathbf{I})). \quad (10)$$

where CE denotes the pixel-wise cross-entropy loss.

3.3 Extending U-KAN to Diffusion Models

The above discussion focuses on generating the segmentation masks given input image \mathbf{I} through the U-KAN. In this section, we further extend U-KAN to a diffusion version, coined Diffusion U-KAN, which unleashes the generative capacity of KANs. Following Denosing Diffusion Probabilistic Models (DDPM) [26], Diffusion U-KAN is able to generate an image from a random Gaussian noise $\epsilon \sim \mathcal{N}(0, 1)$ by gradually removing the noise. This process can be achieved by predicting the noise given a noisy input: $\epsilon_t = \text{U-KAN}(\mathbf{I}_t, t)$, where \mathbf{I}_t is image \mathbf{I} corrupted by Gaussian noise ϵ_t , $t = [1, T]$, $T = 1000$ is the time-step controlling the noise intensity, and $\mathbf{I}_T \sim \mathcal{N}(0, 1)$.

To this end, we conduct two modifications based on the Segmentation U-KAN to lift it to the diffusion version. First, different from only propagating features among different hidden layers, we inject learnable time embedding into each block to enable the network time-aware (see the dashed-line ‘‘Time Embedding’’ in Fig 1) and remove the DwConv and residual connections, thereby changing Eq. 7 into the following format for the goal of generative tasks:

$$\mathbf{Z}_k = \text{LN}(\text{KAN}(\mathbf{Z}_{k-1})) + \mathcal{F}(\text{TE}(t)), \quad (11)$$

where \mathcal{F} is the linear projection, $\text{TE}(t)$ indicates the time embedding for the given time step t [26]. Second, we modify the predicted objective to enable diffusion-based image generation. Instead of

predicting segmented masks given images, Diffusion U-KAN aims to predict the noise ϵ_t given the noise-corrupted image I_t and a random time-step $t = \text{Uniform}(1, T)$, which is optimized via MSE loss as follows:

$$\mathcal{L}_{\text{Diff}} = \|\epsilon_t - \text{U-KAN}(I_t, t)\|_2. \quad (12)$$

After optimization via the above loss function, the DDPM sampling algorithm [26] is used to generate images, which leverages the well-trained Diffusion U-KAN for denoising.

4 Experiments

4.1 Datasets

We conducted a thorough evaluation of our proposed method on three distinct and heterogeneous datasets, each exhibiting unique characteristics, varying data sizes, and disparate image resolutions. These datasets are commonly utilized for tasks such as image segmentation and generation, providing a robust testing ground for the efficacy and adaptability of our method.

BUSI The BUSI dataset [1] is made up of ultrasound images depicting normal, benign, and malignant breast cancer cases along with their corresponding segmentation maps. For our study, we utilized 647 ultrasound images representing both benign and malignant breast tumors. All these images were consistently resized to the dimensions of 256×256 . The dataset offers a comprehensive collection of images that aid in the detection and differentiation of various types of breast tumors, providing valuable insights for medical professionals and researchers.

GlaS The GlaS dataset [80] is comprised of 612 Standard Definition (SD) frames from 31 sequences. Each frame possesses a resolution of 384×288 and was collected from 23 patients. This dataset is associated with the Hospital Clinic located in Barcelona, Spain. The sequences within this dataset were recorded using devices such as Olympus Q160AL and Q165L, coupled with an Extra II video processor. Our study specifically used 165 images from the GlaS dataset, all of which were adjusted to the dimensions of 512×512 .

CVC-ClinicDB The CVC-ClinicDB dataset [5], often abbreviated simply as "CVC," serves as a publicly accessible resource for polyp diagnosis within colonoscopy videos. It encompasses a total of 612 images, each having a resolution of 384×288 , meticulously extracted from 31 distinct colonoscopy sequences. These frames provide a diverse array of polyp instances, making them particularly useful for the development and evaluation of polyp detection algorithms. To ensure consistency across different datasets used in our study, all images from the CVC-ClinicDB dataset were uniformly resized to 256×256 .

4.2 Implementation Details

Segmentation U-KAN We implemented U-KAN using Pytorch on a NVIDIA RTX 4090 GPU. For the BUSI, GlaS and CVC datasets, the batch size was set to 8 and the learning rate was $1e-4$. We used the Adam optimizer to train the model, and used a cosine annealing learning rate scheduler with a minimum learning rate of $1e-5$. The loss function was a combination of binary cross entropy (BCE) and dice loss. We randomly split each dataset into 80% training and 20% validation subsets. All the results among these datasets are reported over three random runs. Only vanilla data augmentations including random rotation and flipping is applied. We trained the model for 400 epochs in total. We compare the output segmentation images both qualitatively and quantitatively using various metrics such as IoU and F1 Score. We also report the metrics related to computation cost such as Gflops and number of parameters (Params).

Diffusion U-KAN The image was cropped and resized into 64×64 for unconditional generation. We benchmark all the methods with the same training setting: $1e-4$ learning rate, 1000 epochs, Adam optimizer, and cosine annealing learning rate scheduler. To evaluate the generation capacity of each method, we generate 2048 image samples using random Gaussian noise as input. We then compare the generated images qualitatively and quantitatively using various metrics such as Fréchet Inception Distance (FID) [65] and Inception Score (IS) [75]. These metrics provide insights into the diversity and quality of the generated images.

4.3 Comparison with State-of-the-arts on Image Segmentation

Table 1 presents the results of the proposed U-KAN against all the compared methods over all the benchmarking datasets. Comparisons between our U-KAN and recently favored frameworks for medical image segmentation were conducted, benchmarking against convolutional baseline models such as U-Net[71], U-Net++[94]. We also evaluated performance against attention-based counterparts including Att-UNet [63] and the state-of-the-art efficient transformer variant, U-Mamba [56]. Furthermore, as KAN emerges as a promising alternative of MLP, we further perform comparison against the advanced MLP-based segmentation networks, including U-Next [81] and Rolling-UNet [54]. In terms of the performance metrics, two standard metrics including Intersection over Union (IoU) and F1 scores are used for evaluating image segmentation tasks. The results demonstrate that across all datasets, our U-KAN surpasses the performance of all other methodologies.

Table 1: Comparison with state-of-the-art segmentation models on three heterogeneous medical scenarios. The average results with standard deviation over three random runs are reported.

| Methods | BUSI [1] | | GlaS [80] | | CVC [5] | |
|-------------------|-------------------|-------------------|-------------------|-------------------|-------------------|-------------------|
| | IoU↑ | F1↑ | IoU↑ | F1↑ | IoU↑ | F1↑ |
| U-Net [71] | 57.22±4.74 | 71.91±3.54 | 86.66±0.91 | 92.79±0.56 | 83.79±0.77 | 91.06±0.47 |
| Att-Unet [63] | 55.18±3.61 | 70.22±2.88 | 86.84±1.19 | 92.89±0.65 | 84.52±0.51 | 91.46±0.25 |
| U-Net++ [94] | 57.41±4.77 | 72.11±3.90 | 87.07±0.76 | 92.96±0.44 | 84.61±1.47 | 91.53±0.88 |
| U-NeXt [81] | 59.06±1.03 | 73.08±1.32 | 84.51±0.37 | 91.55±0.23 | 74.83±0.24 | 85.36±0.17 |
| Rolling-UNet [54] | 61.00±0.64 | 74.67±1.24 | 86.42±0.96 | 92.63±0.62 | 82.87±1.42 | 90.48±0.83 |
| U-Mamba [56] | 61.81±3.24 | 75.55±3.01 | 87.01±0.39 | 93.02±0.24 | 84.79±0.58 | 91.63±0.39 |
| Seg. U-KAN (Ours) | 63.38±2.83 | 76.40±2.90 | 87.64±0.32 | 93.37±0.16 | 85.05±0.53 | 91.88±0.29 |

In addition to the accuracy benefits, this paper further demonstrates the efficiency of our method when used as a network baseline. As shown in Table 2, we report the model’s parameter volume (M) and Gflops on various datasets, as well as segmentation accuracy. The results indicate that our method not only surpasses most segmentation methods in terms of segmentation accuracy, but also exhibits significant advantages or comparable levels in terms of efficiency, with the exception of UNext. Overall, in the trade-off between segmentation accuracy and efficiency, our method exhibits the best performance.

Table 2: Overall comparison with state-of-the-art segmentation models w.r.t. efficiency and segmentation metrics.

| Methods | Average Seg. | | Efficiency | |
|-------------------|-------------------|-------------------|------------|------------|
| | IoU↑ | F1↑ | Gflops | Params (M) |
| U-Net [71] | 75.89±2.14 | 85.25±1.52 | 524.2 | 34.53 |
| Att-Unet [63] | 75.51±1.77 | 84.85±1.26 | 533.1 | 34.9 |
| U-Net++ [94] | 76.36±2.33 | 85.53±1.74 | 1109 | 36.6 |
| U-NeXt [81] | 72.80±0.54 | 83.33±0.57 | 4.58 | 1.47 |
| Rolling-UNet [54] | 76.76±1.01 | 85.92±0.89 | 16.82 | 1.78 |
| U-Mamba [56] | 77.87±1.47 | 86.73±1.25 | 2087 | 86.3 |
| Seg. U-KAN (Ours) | 78.69±1.27 | 87.22±1.15 | 14.02 | 6.35 |

We further present a comprehensive qualitative comparison across all datasets, as depicted in Figure 2. Firstly, it is evident from the results that pure CNN-based approaches such as U-Net and U-Net++ are more prone to over- or under-segmentation of organs, suggesting the limitation of these models in encoding global context and discriminating semantics. In contrast, our proposed U-KAN yields fewer false positives compared to other methods, indicating its superiority in suppressing noisy predictions. When juxtaposed with models based on Transformers, and efficient MLP-based architectures, the predictions of U-KAN often exhibit finer details in terms of boundaries and shapes. These observations underscore U-KAN’s capability for refined segmentation while preserving intricate shape information. This further corroborates our initial intuition, highlighting the advantages introduced by incorporating the KAN layer.

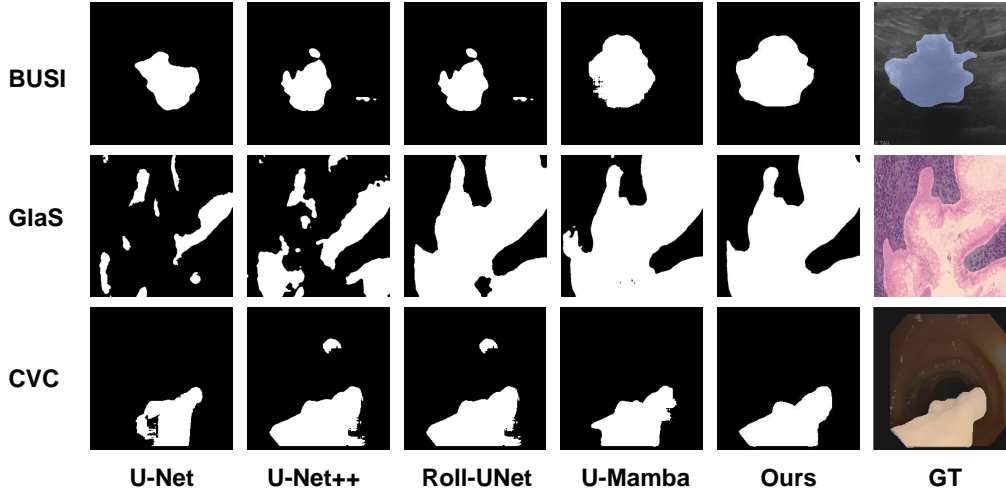


Figure 2: Visualized segmentation results of the proposed U-KAN against other state-of-the-arts over three heterogeneous medical scenarios.

4.4 Comparison with State-of-the-arts on Image Generation

We investigated the potential of our proposed U-KAN as a backbone for generative tasks. We compared our U-KAN with various diffusion variant models, all based on conventional U-Nets, in order to evaluate the efficacy of this architecture for different generative tasks. The results were presented in Table 3, where we reported FID [65] (Fréchet Inception Distance) and IS [75] (Inception Score) metrics across three datasets. The Fréchet Inception Distance is a measure of the distance between two distributions, in this case, between the distribution of generated images and the distribution of real images. The lower the FID, the better the generated images resemble the real images. On the other hand, the Inception Score measures the quality of the generated images by evaluating how well these images can be classified into specific categories. The higher the IS, the better the generated images are classified correctly. The results from our experiments clearly indicate that our method exhibits superior generative performance compared to other state-of-the-art models in the field. This suggests that the architecture of our U-KAN is particularly suitable for generative tasks, providing an effective and efficient approach to generating high-quality images.

Table 3: Comparison with standard U-Net based diffusion models on three heterogeneous medical scenarios. Results by different variants of Diffusion U-Net is provided for comprehensive evaluation.

| Methods | Middle Blocks | BUSI [1] | | GlaS [80] | | CVC [5] | |
|------------------------|---------------|---------------|-------------|--------------|-------------|--------------|-------------|
| | | FID↓ | IS↑ | FID↓ | IS↑ | FID↓ | IS↑ |
| Diffusion U-Net | ResBlock+Attn | 116.52 | 2.54 | 42.65 | 2.45 | 49.30 | 2.65 |
| | Identity | 124.46 | 2.71 | 42.63 | 2.41 | 50.42 | 2.49 |
| | MLP | 104.95 | 2.59 | 44.21 | 2.43 | 51.16 | 2.69 |
| Diffusion U-KAN (Ours) | KANBlock | 101.93 | 2.76 | 41.55 | 2.46 | 46.34 | 2.75 |

Figure 3 displays visualizations of some of our generated results. It is observed that our method can produce realistic and diverse content across multiple distinct datasets, demonstrating its versatility and effectiveness in generating high-quality images. This further supports the claim that U-KAN has a significant advantage when it comes to generative tasks, making it a strong candidate for future research and development in this area.

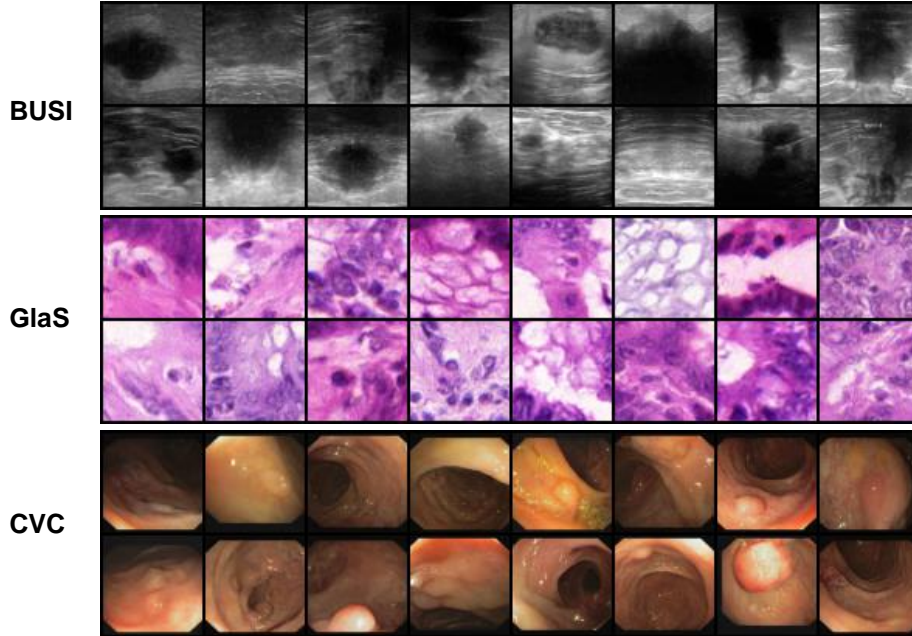


Figure 3: Generated images given by Diffusion U-KAN in three heterogeneous medical scenarios.

4.5 Ablation Studies

To thoroughly evaluate the proposed TransUNet framework and validate the performance under different settings, a variety of ablation studies were performed as follows.

The Number of KAN Layer As previously stated, the inclusion of KAN Layers in U-KAN has proven beneficial by facilitating the modeling of more refined segmentation details through the explicit incorporation of highly efficient embeddings. The objective of this ablation study was to assess the impact of incorporating varying quantities of KAN Layers. We modified the number of KAN Layers from one to five, as depicted in Table 4. It is observed that the configuration with three KAN Layers yielded the most superior performance. These outcomes corroborate our initial hypothesis that the strategic integration of an adequate number of KAN Layers within the U-KAN can effectively capture intricate segmentation-related nuances.

Impact on Using KAN Layer v.s. MLP To further substantiate the role of KAN layers in enhancing model performance, we conducted an array of ablation experiments, as shown in Table 5. In these experiments, we replaced the introduced KAN layers with traditional multilayer perceptrons (MLPs) to observe if such modifications would result in a decrease in performance. This methodology allowed us to more tangibly comprehend the significance of KAN layers in improving both the model’s interpretability and its overall performance. Initially, we modified a model that already incorporated KAN layers, replacing one or several KAN layers with standard MLPs. Subsequently, using identical datasets and training parameters, we retrained the modified model and documented its performance across various tasks. The outcomes demonstrated a noticeable decline in performance across multiple tasks when KAN layers were replaced with MLPs, particularly in intricate tasks requiring robust feature extraction and representational capacities. These findings underscore the crucial role of KAN layers in augmenting the model’s expressive capabilities and bolstering its overall performance.

Model Scaling Lastly, we conducted an ablation study on various model sizes of the U-KAN. Specifically, we examined alternative configurations of the U-KAN, termed as *Small* and *Large* models. The primary distinction between these variants lies in their channel settings, denoted as the

Table 4: Ablation studies on number of used KAN layers. The default setup is denoted.

| #KAN | IoU \uparrow | F1 \uparrow | Gflops |
|---------|----------------|---------------|--------|
| 1 Layer | 64.20 | 77.81 | 13.97 |
| 2 Layer | 64.56 | 78.01 | 14.00 |
| 3 Layer | 66.65 | 79.75 | 14.02 |
| 4 Layer | 66.28 | 79.44 | 14.05 |
| 5 Layer | 64.86 | 78.42 | 14.07 |

Table 5: Ablation studies on using KAN layers against MLPs. The default setup is denoted.

| KAN or MLP? | IoU \uparrow | F1 \uparrow | Gflops |
|----------------|----------------|---------------|--------|
| KAN \times 3 | 66.65 | 79.75 | 14.02 |
| MLP+KAN+KAN | 62.07 | 76.06 | 14.29 |
| KAN+MLP+KAN | 63.82 | 77.58 | 14.29 |
| KAN+KAN+MLP | 62.50 | 76.32 | 14.29 |
| MLP \times 3 | 61.06 | 75.63 | 14.84 |

varied channel number from first to third KAN layer (C_1 - C_3), as detailed in Table 6. The *Small* model features channel settings of 64-96-128, while the *Large* model’s channel counts are set to 256-320-512. In contrast, our default model’s channel numbers are configured at 128-160-256. We observed that larger models correlate with enhanced performance, which aligns with the scaling law characteristics exhibited by models integrating KAN. Ultimately, to strike a balance between performance and computational expenses, we opted to employ the default base model in our experiments.

Table 6: Ablation studies on model scaling by using different channel settings in U-KAN. The default setup is denoted.

| Model Scale | C_1 | C_2 | C_3 | IoU \uparrow | F1 \uparrow | Gflops |
|-------------|-------|-------|-------|----------------|---------------|--------|
| U-KAN-S | 64 | 96 | 128 | 64.62 | 78.28 | 3.740 |
| U-KAN | 128 | 160 | 256 | 66.65 | 79.75 | 14.02 |
| U-KAN-L | 256 | 320 | 512 | 66.81 | 79.99 | 55.11 |

5 Conclusion

This paper introduces U-KAN and demonstrates the significant potential of Kolmogorov-Arnold Networks (KANs) in enhancing backbones like U-Net for various visual applications. By integrating KAN layers into the U-Net architecture, you can make a strong network for vision tasks in terms of impressive accuracy, efficiency and interpretability. We perform empirical evaluations of our method under several medical image segmentation tasks. Moreover, the adaptability and effectiveness of U-KAN also highlight its potential as a superior alternative to U-Net for noise prediction in diffusion models. These findings underscore the importance of exploring non-traditional network structures like KANs for advancing a broader range of vision applications.

References

- [1] Walid Al-Dhabyani, Mohammed Gomaa, Hussien Khaled, and Aly Fahmy. Dataset of breast ultrasound images. *Data in brief*, 28:104863, 2020.
- [2] Simon Andermatt, Simon Pezold, and Philippe C Cattin. Multi-dimensional gated recurrent units for the segmentation of biomedical 3d-data. In *Deep Learning and Data Labeling for Medical Applications*, pages 142–151. Springer, Cham, 2016.
- [3] Omri Avrahami, Dani Lischinski, and Ohad Fried. Blended diffusion for text-driven editing of natural images. In *Proc. of IEEE Intl. Conf. on Computer Vision and Pattern Recognition*, 2022.
- [4] Jimmy Lei Ba, Jamie Ryan Kiros, and Geoffrey E Hinton. Layer normalization. *arXiv preprint arXiv:1607.06450*, 2016.
- [5] Jorge Bernal, F Javier Sánchez, Gloria Fernández-Esparrach, Debora Gil, Cristina Rodríguez, and Fernando Vilariño. Wm-dova maps for accurate polyp highlighting in colonoscopy: Validation vs. saliency maps from physicians. *Computerized medical imaging and graphics*, 43:99–111, 2015.
- [6] Andreas Blattmann, Robin Rombach, Huan Ling, Tim Dockhorn, Seung Wook Kim, Sanja Fidler, and Karsten Kreis. Align your latents: High-resolution video synthesis with latent diffusion models. In *Proc. of IEEE Intl. Conf. on Computer Vision and Pattern Recognition*, 2023.

- [7] Andrew Brock, Jeff Donahue, and Karen Simonyan. Large scale GAN training for high fidelity natural image synthesis. *arXiv preprint arXiv:1809.11096*, 2018.
- [8] Jinming Cao, Yangyan Li, Mingchao Sun, Ying Chen, Dani Lischinski, Daniel Cohen-Or, Baoquan Chen, and Changhe Tu. Do-conv: Depthwise over-parameterized convolutional layer. *IEEE Transactions on Image Processing*, 31:3726–3736, 2022.
- [9] Jieneng Chen, Yongyi Lu, Qihang Yu, Xiangde Luo, Ehsan Adeli, Yan Wang, Le Lu, Alan L Yuille, and Yuyin Zhou. Transunet: Transformers make strong encoders for medical image segmentation. *arXiv preprint arXiv:2102.04306*, 2021.
- [10] Yinda Chen, Haoyuan Shi, Xiaoyu Liu, Te Shi, Ruobing Zhang, Dong Liu, Zhiwei Xiong, and Feng Wu. Tokenunify: Scalable autoregressive visual pre-training with mixture token prediction. *arXiv preprint arXiv:2405.16847*, 2024.
- [11] Jooyoung Choi, Sungwon Kim, Yonghyun Jeong, Youngjune Gwon, and Sungroh Yoon. Ilvr: Conditioning method for denoising diffusion probabilistic models. *arXiv preprint arXiv:2108.02938*, 2021.
- [12] Özgün Çiçek, Ahmed Abdulkadir, Soeren S Lienkamp, Thomas Brox, and Olaf Ronneberger. 3d u-net: learning dense volumetric segmentation from sparse annotation. In *Medical Image Computing and Computer-Assisted Intervention–MICCAI 2016: 19th International Conference, Athens, Greece, October 17–21, 2016, Proceedings, Part II 19*, pages 424–432. Springer, 2016.
- [13] Zhiyuan Ding, Qi Dong, Haote Xu, Chenxin Li, Xinghao Ding, and Yue Huang. Unsupervised anomaly segmentation for brain lesions using dual semantic-manifold reconstruction. In *International Conference on Neural Information Processing*, pages 133–144. Springer, 2022.
- [14] Alexey Dosovitskiy, Lucas Beyer, Alexander Kolesnikov, Dirk Weissenborn, Xiaohua Zhai, Thomas Unterthiner, Mostafa Dehghani, Matthias Minderer, Georg Heigold, Sylvain Gelly, et al. An image is worth 16x16 words: Transformers for image recognition at scale. In *Proc. of Intl. Conf. on Learning Representations*, 2021.
- [15] Patrick Esser, Robin Rombach, and Bjorn Ommer. Taming transformers for high-resolution image synthesis. In *Proc. of IEEE Intl. Conf. on Computer Vision and Pattern Recognition*, 2021.
- [16] Daniel Y Fu, Tri Dao, Khaled K Saab, Armin W Thomas, Atri Rudra, and Christopher Ré. Hungry hungry hippos: Towards language modeling with state space models. *arXiv preprint arXiv:2212.14052*, 2022.
- [17] Ian J Goodfellow, Jean Pouget-Abadie, Mehdi Mirza, Bing Xu, David Warde-Farley, Sherjil Ozair, Aaron C Courville, and Yoshua Bengio. Generative adversarial nets. In *Proc. of Advances in Neural Information Processing Systems*, 2014.
- [18] Albert Gu and Tri Dao. Mamba: Linear-time sequence modeling with selective state spaces. *arXiv preprint arXiv:2312.00752*, 2023.
- [19] Albert Gu, Karan Goel, Ankit Gupta, and Christopher Ré. On the parameterization and initialization of diagonal state space models. In *Proc. of Advances in Neural Information Processing Systems*, 2022.
- [20] Zongwei Gu, Jianwen Cheng, Hao Fu, Kai Zhou, Huazhu Hao, Yue Zhao, Tao Zhang, Shuo Gao, and Jianming Liu. Ce-net: Context encoder network for 2d medical image segmentation. *IEEE transactions on medical imaging*, 38(10):2281–2292, 2019.
- [21] Ankit Gupta, Albert Gu, and Jonathan Berant. Diagonal state spaces are as effective as structured state spaces. In *Proc. of Advances in Neural Information Processing Systems*, 2022.
- [22] Ali Hatamizadeh, Vishwesh Nath, Yucheng Tang, Dong Yang, Holger R Roth, and Daguang Xu. Swin unetr: Swin transformers for semantic segmentation of brain tumors in mri images. In *International MICCAI Brainlesion Workshop*, pages 272–284. Springer, 2021.
- [23] Ali Hatamizadeh, Yucheng Tang, Vishwesh Nath, Dong Yang, Andriy Myronenko, Bennett Landman, Holger R Roth, and Daguang Xu. Unetr: Transformers for 3d medical image segmentation. In *Proceedings of the IEEE/CVF winter conference on applications of computer vision*, pages 574–584, 2022.
- [24] Ali Hatamizadeh, Hongxu Yin, Greg Heinrich, Jan Kautz, and Pavlo Molchanov. Global context vision transformers. In *International Conference on Machine Learning*, pages 12633–12646. PMLR, 2023.
- [25] Yingqing He, Tianyu Yang, Yong Zhang, Ying Shan, and Qifeng Chen. Latent video diffusion models for high-fidelity video generation with arbitrary lengths. *arXiv preprint arXiv:2211.13221*, 2022.
- [26] Jonathan Ho, Ajay Jain, and Pieter Abbeel. Denoising diffusion probabilistic models. In *Proc. of Advances in Neural Information Processing Systems*, 2020.
- [27] Wenyi Hong, Ming Ding, Wendi Zheng, Xinghan Liu, and Jie Tang. CogVideo: Large-scale pretraining for text-to-video generation via transformers. *arXiv preprint arXiv:2205.15868*,

- 2022.
- [28] Kurt Hornik, Maxwell Stinchcombe, and Halbert White. Multilayer feedforward networks are universal approximators. *Neural networks*, 2(5):359–366, 1989.
 - [29] Guang-Bin Huang, Lei Zhao, and Yong Song. Deep architecture of kolmogorov-arnold representation. In *2014 International Joint Conference on Neural Networks (IJCNN)*, pages 1001–1008. IEEE, 2014.
 - [30] Guang-Bin Huang, Lei Zhao, and Yuyun Xing. Towards theory of deep learning on graphs: Optimization landscape and train ability of kolmogorov-arnold representation. *Neurocomputing*, 251:10–21, 2017.
 - [31] Hao Huang, Liang Lin, Ruofeng Tong, Hao Hu, Qingsong Zhang, Yutaro Iwamoto, Xiangyue Han, Yutong-L Chen, and Weiyao Xu. Unet 3+: A full-scale connected unet for medical image segmentation. In *2020 IEEE International Conference on Acoustics, Speech and Signal Processing (ICASSP)*, pages 1055–1059. IEEE, 2020.
 - [32] Fabian Isensee, Paul F Jaeger, Simon AA Kohl, Jens Petersen, and Klaus H Maier-Hein. nnu-net: a self-configuring method for deep learning-based biomedical image segmentation. *Nature methods*, 18(2):203–211, 2021.
 - [33] Allan Jabri, David J. Fleet, and Ting Chen. Scalable adaptive computation for iterative generation. *arXiv preprint arXiv:2212.11972*, 2022.
 - [34] Konstantinos Kamnitsas, Christian Ledig, Virginia F Newcombe, Joanna P Simpson, Andrew D Kane, David K Menon, Daniel Rueckert, and Ben Glocker. Efficient multi-scale 3d cnn with fully connected crf for accurate brain lesion segmentation. *Medical image analysis*, 36:61–78, 2017.
 - [35] Tero Karras, Timo Aila, Samuli Laine, and Jaakko Lehtinen. Progressive growing of GANs for improved quality, stability, and variation. In *Proc. of Intl. Conf. on Learning Representations*, 2018.
 - [36] Diederik P Kingma and Max Welling. Auto-encoding variational bayes. *arXiv preprint arXiv:1312.6114*, 2013.
 - [37] Andrey Nikolaevich Kolmogorov. On the representation of continuous functions of many variables by superposition of continuous functions of one variable and addition. *American Mathematical Society Translations*, 28:55–59, 1957.
 - [38] Andrei Nikolaevich Kolmogorov. *On the representation of continuous functions of several variables by superpositions of continuous functions of a smaller number of variables*. American Mathematical Society, 1961.
 - [39] Chenxin Li, Mingbao Lin, Zhiyuan Ding, Nie Lin, Yihong Zhuang, Yue Huang, Xinghao Ding, and Liujuan Cao. Knowledge condensation distillation. In *European Conference on Computer Vision*, pages 19–35. Springer, 2022.
 - [40] Chenxin Li, Xin Lin, Yijin Mao, Wei Lin, Qi Qi, Xinghao Ding, Yue Huang, Dong Liang, and Yizhou Yu. Domain generalization on medical imaging classification using episodic training with task augmentation. *Computers in biology and medicine*, 141:105144, 2022.
 - [41] Chenxin Li, Hengyu Liu, Yifan Liu, Brandon Y Feng, Wuyang Li, Xinyu Liu, Zhen Chen, Jing Shao, and Yixuan Yuan. Endora: Video generation models as endoscopy simulators. *arXiv preprint arXiv:2403.11050*, 2024.
 - [42] Chenxin Li, Wenao Ma, Liyan Sun, Xinghao Ding, Yue Huang, Guisheng Wang, and Yizhou Yu. Hierarchical deep network with uncertainty-aware semi-supervised learning for vessel segmentation. *Neural Computing and Applications*, pages 1–14.
 - [43] Chenxin Li, Yunlong Zhang, Jiongcheng Li, Yue Huang, and Xinghao Ding. Unsupervised anomaly segmentation using image-semantic cycle translation. *arXiv preprint arXiv:2103.09094*, 2021.
 - [44] Chenxin Li, Yunlong Zhang, Zhehan Liang, Wenao Ma, Yue Huang, and Xinghao Ding. Consistent posterior distributions under vessel-mixing: a regularization for cross-domain retinal artery/vein classification. In *2021 IEEE International Conference on Image Processing (ICIP)*, pages 61–65. IEEE, 2021.
 - [45] Zhenglin Li, Bo Guan, Yuanzhou Wei, Yiming Zhou, Jingyu Zhang, and Jinxin Xu. Mapping new realities: Ground truth image creation with pix2pix image-to-image translation. *arXiv preprint arXiv:2404.19265*, 2024.
 - [46] Zhenglin Li, Yangchen Huang, Mengran Zhu, Jingyu Zhang, JingHao Chang, and Houze Liu. Feature manipulation for ddpm based change detection. *arXiv preprint arXiv:2403.15943*, 2024.
 - [47] Xi Liang, Lei Zhao, and Guang-Bin Huang. Deep kolmogorov-arnold representation for learning dynamics. *IEEE Access*, 6:49436–49446, 2018.
 - [48] Xinyu Liu, Xiaoqing Guo, Yajie Liu, and Yixuan Yuan. Consolidated domain adaptive detection and localization framework for cross-device colonoscopic images. *Medical image analysis*,

- 71:102052, 2021.
- [49] Xinyu Liu, Wuyang Li, and Yixuan Yuan. Decoupled unbiased teacher for source-free domain adaptive medical object detection. *IEEE Transactions on Neural Networks and Learning Systems*, 2023.
- [50] Xinyu Liu, Houwen Peng, Ningxin Zheng, Yuqing Yang, Han Hu, and Yixuan Yuan. Efficientvit: Memory efficient vision transformer with cascaded group attention. In *Proceedings of the IEEE/CVF Conference on Computer Vision and Pattern Recognition*, pages 14420–14430, 2023.
- [51] Xinyu Liu and Yixuan Yuan. A source-free domain adaptive polyp detection framework with style diversification flow. *IEEE Transactions on Medical Imaging*, 41(7):1897–1908, 2022.
- [52] Yifan Liu, Chenxin Li, Chen Yang, and Yixuan Yuan. Endogaussian: Gaussian splatting for deformable surgical scene reconstruction. *arXiv preprint arXiv:2401.12561*, 2024.
- [53] Yue Liu, Yunjie Tian, Yuzhong Zhao, Hongtian Yu, Lingxi Xie, Yaowei Wang, Qixiang Ye, and Yunfan Liu. Vmamba: Visual state space model. *arXiv preprint arXiv:2401.10166*, 2024.
- [54] Yutong Liu, Haijiang Zhu, Mengting Liu, Huaiyuan Yu, Zihan Chen, and Jie Gao. Rolling-unet: Revitalizing mlp’s ability to efficiently extract long-distance dependencies for medical image segmentation. In *Proceedings of the AAAI Conference on Artificial Intelligence*, volume 38, pages 3819–3827, 2024.
- [55] Ziming Liu, Yixuan Wang, Sachin Vaidya, Fabian Ruehle, James Halverson, Marin Soljačić, Thomas Y Hou, and Max Tegmark. Kan: Kolmogorov-arnold networks. *arXiv preprint arXiv:2404.19756*, 2024.
- [56] Jun Ma, Feifei Li, and Bo Wang. U-mamba: Enhancing long-range dependency for biomedical image segmentation. *arXiv preprint arXiv:2401.04722*, 2024.
- [57] Harsh Mehta, Ankit Gupta, Ashok Cutkosky, and Behnam Neyshabur. Long range language modeling via gated state spaces. In *Proc. of Intl. Conf. on Learning Representations*, 2022.
- [58] Sachin Mehta, Ezgi Mercan, Jamen Bartlett, Donald Weaver, Joann G Elmore, and Linda Shapiro. Y-net: joint segmentation and classification for diagnosis of breast biopsy images. In *Medical Image Computing and Computer Assisted Intervention–MICCAI 2018: 21st International Conference, Granada, Spain, September 16–20, 2018, Proceedings, Part II 11*, pages 893–901. Springer, 2018.
- [59] Chenlin Meng, Yutong He, Yang Song, Jiaming Song, Jiajun Wu, Jun-Yan Zhu, and Stefano Ermon. SDEdit: Guided image synthesis and editing with stochastic differential equations. In *Proc. of Intl. Conf. on Learning Representations*, 2022.
- [60] Fausto Milletari, Nassir Navab, and Seyed-Ahmad Ahmadi. V-net: Fully convolutional neural networks for volumetric medical image segmentation. In *2016 fourth international conference on 3D vision (3DV)*, pages 565–571. Ieee, 2016.
- [61] Mehdi Mirza and Simon Osindero. Conditional generative adversarial nets. *arXiv preprint arXiv:1411.1784*, 2014.
- [62] Andriy Myronenko. 3d mri brain tumor segmentation using autoencoder regularization. In *Brainlesion: Glioma, Multiple Sclerosis, Stroke and Traumatic Brain Injuries: 4th International Workshop, BrainLes 2018, Held in Conjunction with MICCAI 2018, Granada, Spain, September 16, 2018, Revised Selected Papers, Part II 4*, pages 311–320. Springer, 2019.
- [63] Ozan Oktay, Jo Schlemper, Loic Le Folgoc, Matthew Lee, Mattias Heinrich, Kazunari Misawa, Kensaku Mori, Steven McDonagh, Nils Y Hammerla, Bernhard Kainz, et al. Attention u-net: Learning where to look for the pancreas. *arXiv preprint arXiv:1804.03999*, 2018.
- [64] Druv Pai, Sam Buchanan, Ziyang Wu, Yaodong Yu, and Yi Ma. Masked completion via structured diffusion with white-box transformers. In *The Twelfth International Conference on Learning Representations*, 2024.
- [65] Gaurav Parmar, Richard Zhang, and Jun-Yan Zhu. On buggy resizing libraries and surprising subtleties in fid calculation. *arXiv preprint arXiv:2104.11222*, 5:14, 2021.
- [66] William Peebles and Saining Xie. Scalable diffusion models with transformers. In *Proceedings of the IEEE/CVF International Conference on Computer Vision*, pages 4195–4205, 2023.
- [67] Bo Peng, Eric Alcaide, Quentin Anthony, Alon Albalak, Samuel Arcadinho, Stella Biderman, Huanqi Cao, Xin Cheng, Michael Chung, Matteo Grella, et al. Rwkv: Reinventing rnns for the transformer era. *arXiv preprint arXiv:2305.13048*, 2023.
- [68] Maithra Raghu, Thomas Unterthiner, Simon Kornblith, Chiyuan Zhang, and Alexey Dosovitskiy. Do vision transformers see like convolutional neural networks? *Advances in Neural Information Processing Systems*, 34:12116–12128, 2021.
- [69] Aditya Ramesh, Prafulla Dhariwal, Alex Nichol, Casey Chu, and Mark Chen. Hierarchical text-conditional image generation with CLIP latents. *arXiv preprint arXiv:2204.06125*, 2022.

- [70] Robin Rombach, Andreas Blattmann, Dominik Lorenz, Patrick Esser, and Björn Ommer. High-resolution image synthesis with latent diffusion models. In *Proc. of IEEE Intl. Conf. on Computer Vision and Pattern Recognition*, 2022.
- [71] Olaf Ronneberger, Philipp Fischer, and Thomas Brox. U-net: Convolutional networks for biomedical image segmentation. *International Conference on Medical image computing and computer-assisted intervention*, pages 234–241, 2015.
- [72] Jiacheng Ruan and Suncheng Xiang. Vm-unet: Vision mamba unet for medical image segmentation. *arXiv preprint arXiv:2402.02491*, 2024.
- [73] Chitwan Saharia, William Chan, Huiwen Chang, Chris Lee, Jonathan Ho, Tim Salimans, David Fleet, and Mohammad Norouzi. Palette: Image-to-image diffusion models. 2022.
- [74] Chitwan Saharia, William Chan, Saurabh Saxena, Lala Li, Jay Whang, Emily Denton, Seyed Kamyar Seyed Ghasemipour, Burcu Karagol Ayan, S Sara Mahdavi, Rapha Gontijo Lopes, et al. Photorealistic text-to-image diffusion models with deep language understanding. *arXiv preprint arXiv:2205.11487*, 2022.
- [75] Masaki Saito, Eiichi Matsumoto, and Shunta Saito. Temporal generative adversarial nets with singular value clipping. In *Proceedings of the IEEE international conference on computer vision*, pages 2830–2839, 2017.
- [76] Jo Schlemper, Ozan Oktay, Michiel Schaap, Mattias Heinrich, Bernhard Kainz, Ben Glocker, and Daniel Rueckert. Attention gated networks: Learning to leverage salient regions in medical images. *Medical image analysis*, 53:197–207, 2019.
- [77] Dinggang Shen, Guorong Wu, and Heung-Il Suk. Deep learning in medical image analysis. *Annual review of biomedical engineering*, 19:221–248, 2017.
- [78] Liyan Sun, Chenxin Li, Xinghao Ding, Yue Huang, Zhong Chen, Guisheng Wang, Yizhou Yu, and John Paisley. Few-shot medical image segmentation using a global correlation network with discriminative embedding. *Computers in biology and medicine*, 140:105067, 2022.
- [79] Hugo Touvron, Matthieu Cord, Matthijs Douze, Francisco Massa, Alexandre Sablayrolles, and Hervé Jégou. Training data-efficient image transformers & distillation through attention. In *International conference on machine learning*, pages 10347–10357. PMLR, 2021.
- [80] Jeya Maria Jose Valanarasu, Poojan Oza, Ilker Hacihaliloglu, and Vishal M Patel. Medical transformer: Gated axial-attention for medical image segmentation. In *Medical Image Computing and Computer Assisted Intervention—MICCAI 2021: 24th International Conference, Strasbourg, France, September 27–October 1, 2021, Proceedings, Part I 24*, pages 36–46. Springer, 2021.
- [81] Jeya Maria Jose Valanarasu and Vishal M Patel. Unext: Mlp-based rapid medical image segmentation network. In *International conference on medical image computing and computer-assisted intervention*, pages 23–33. Springer, 2022.
- [82] Aaron Van Den Oord, Oriol Vinyals, et al. Neural discrete representation learning. In *Proc. of Advances in Neural Information Processing Systems*, 2017.
- [83] Pei Wang, Yijun Li, and Nuno Vasconcelos. Rethinking and improving the robustness of image style transfer. In *Proceedings of the IEEE/CVF conference on computer vision and pattern recognition*, pages 124–133, 2021.
- [84] Risheng Wang, Tao Lei, Ruixia Cui, Bingtao Zhang, Hongying Meng, and Asoke K Nandi. Medical image segmentation using deep learning: A survey. *IET Image Processing*, 16(5):1243–1267, 2022.
- [85] Tengfei Wang, Ting Zhang, Bo Zhang, Hao Ouyang, Dong Chen, Qifeng Chen, and Fang Wen. Pretraining is all you need for image-to-image translation. *arXiv preprint arXiv:2205.12952*, 2022.
- [86] Enze Xie, Wenhai Wang, Zhiding Yu, Anima Anandkumar, Jose M Alvarez, and Ping Luo. Segformer: Simple and efficient design for semantic segmentation with transformers. *Advances in neural information processing systems*, 34:12077–12090, 2021.
- [87] Yuyun Xing, Lei Zhao, and Guang-Bin Huang. Kolmogorov-arnold representation based deep learning for time series forecasting. In *2018 IEEE Symposium Series on Computational Intelligence (SSCI)*, pages 1483–1490. IEEE, 2018.
- [88] Zhaohu Xing, Tian Ye, Yijun Yang, Guang Liu, and Lei Zhu. Segmamba: Long-range sequential modeling mamba for 3d medical image segmentation. *arXiv preprint arXiv:2401.13560*, 2024.
- [89] Haipeng Xu, Chenxin Li, Longfeng Zhang, Zhiyuan Ding, Tao Lu, and Huihua Hu. Immunotherapy efficacy prediction through a feature re-calibrated 2.5 d neural network. *Computer Methods and Programs in Biomedicine*, 249:108135, 2024.
- [90] Haote Xu, Yunlong Zhang, Liyan Sun, Chenxin Li, Yue Huang, and Xinghao Ding. Afsc: Adaptive fourier space compression for anomaly detection. *arXiv preprint arXiv:2204.07963*, 2022.

- [91] Runzhao Yang, Yinda Chen, Zhihong Zhang, Xiaoyu Liu, Zongren Li, Kunlun He, Zhiwei Xiong, Jinli Suo, and Qionghai Dai. Unicompress: Enhancing multi-data medical image compression with knowledge distillation. *arXiv preprint arXiv:2405.16850*, 2024.
- [92] Yaodong Yu, Sam Buchanan, Druv Pai, Tianzhe Chu, Ziyang Wu, Shengbang Tong, Benjamin Haeffele, and Yi Ma. White-box transformers via sparse rate reduction. *Advances in Neural Information Processing Systems*, 36, 2024.
- [93] Yunlong Zhang, Chenxin Li, Xin Lin, Liyan Sun, Yihong Zhuang, Yue Huang, Xinghao Ding, Xiaoqing Liu, and Yizhou Yu. Generator versus segmentor: Pseudo-healthy synthesis. In *Medical Image Computing and Computer Assisted Intervention—MICCAI 2021: 24th International Conference, Strasbourg, France, September 27–October 1, 2021, Proceedings, Part VI 24*, pages 150–160. Springer, 2021.
- [94] Zongwei Zhou, Md Mahfuzur Rahman Siddiquee, Nima Tajbakhsh, and Jianming Liang. Unet++: A nested u-net architecture for medical image segmentation. In *Deep learning in medical image analysis and multimodal learning for clinical decision support*, pages 3–11. Springer, Cham, 2018.
- [95] Lianghai Zhu, Bencheng Liao, Qian Zhang, Xinlong Wang, Wenyu Liu, and Xinggang Wang. Vision mamba: Efficient visual representation learning with bidirectional state space model. *arXiv preprint arXiv:2401.09417*, 2024.